Journal of Smart Farming and Food Security
Universiti Malaysia Sabah, Malaysia

EVALUATING THE VERTICAL ACCURACY OF LIDAR AND OPEN-SOURCE DEM FOR OIL PALM PLANTATION PLANNING AND DESIGN

Alfred Michael Sikab, Wilson V. C. Wong

Faculty of Tropical Forestry, UMS
*Corresponding author: alfredmichael76@gmail.com

Abstract:
Accurate elevation data are essential for effective oil palm plantation planning, hydrological modeling, and environmental management particularly in tropical regions characterized by complex topography and dense vegetation. While LiDAR-derived Digital Elevation Models (DEMs) offer high vertical precision, their acquisition costs often hinder adoption in resource-limited settings. Open-source DEMs provide accessible alternatives but are frequently affected by vegetation interference and coarse resolution, leading to reduced vertical accuracy. This study proposes a hybrid correction framework that integrates a random forest (RF) machine learning algorithm and a geographically weighted regression (GWR) a spatially adaptive statistical method to enhance the vertical accuracy of open-source DEMs for terrain-sensitive applications. The study used 377 high-precision Ground Control Points (GCPs) and LiDAR data to evaluate and correct six global DEMs: Advanced Land Observing Satellite (ALOS), TerraSAR-X add-on for Digital Elevation Measurement (TanDEM-X), Copernicus GLO-30, Shuttle Radar Topography Mission (SRTM), Forest And Buildings removed Copernicus DEM (FABDEM), Advanced Spaceborne Thermal Emission and Reflection Radiometer (ASTER) GDEM, and a high-resolution drone-derived DEM. RF was used to identify key topographic predictors, including aspect, slope, curvature, Topographic Position Index (TPI), and Terrain Ruggedness Index (TRI), while GWR applied spatially adaptive corrections to the RF residuals. The integrated RF–GWR model significantly improved the vertical accuracy across all DEMs. The post-correction R^2 values reached 0.914 for TanDEM-X, 0.910 for ALOS, and increased from 0.608 to 0.914 for Copernicus, with the residual standard deviations reduced by up to 75% and near-zero mean bias. These results highlight the model's ability to correct both systematic and spatially varying elevation errors. The framework presents a scalable and alternative to LiDAR for use in precision agriculture, flood risk modeling, and infrastructure planning. Future work should explore integration with deep learning to improve the temporal responsiveness and operational scalability.

Keywords: Digital Elevation Models, Machine Learning, Random Forest, Geographically Weighted Regression, Vertical Accuracy.

1. INTRODUCTION

Accurate terrain data are fundamental to informed land-use planning, hydrological modeling, and precision agriculture, particularly in tropical environments characterized by dense vegetation, high rainfall, and complex topography. In the context of oil palm plantation development, reliable elevation models are critical for the design of efficient drainage systems, optimization of

plantation infrastructure, and mitigation of erosion and flooding risks. DEMs play a central role in these applications, yet their utility depends heavily on vertical accuracy, which varies considerably across different data sources and landscape conditions (Chai et al., 2022; Karlson et al., 2021). LiDAR-derived DEMs are widely regarded as the benchmark for high-precision topographic representation, often achieving sub-meter vertical accuracy and fine spatial resolution. However, the high financial and logistical costs associated with LiDAR acquisition and processing limit their widespread adoption, especially in large-scale or resource-constrained agricultural operations (Mohamed, 2020; Tavares da Costa et al., 2019). As a result, freely available open-source DEMs such as ALOS AW3D30, ASTER GDEM, Copernicus GLO-30, FABDEM, SRTM, and TanDEM-X are commonly utilized due to their global coverage and ease of access. Nevertheless, these datasets frequently exhibit vertical inaccuracies caused by vegetation interference, coarse resolution, and limitations in sensor technology issues that are especially pronounced in tropical plantation landscapes (MARTINEZ, 2020; Tabunshchik et al., 2023).

Although numerous studies have assessed the accuracy of global DEMs, several critical gaps persist in the literature. First, existing evaluations are often generalized at the national or continental scales, thereby overlooking the fine-resolution accuracy requirements necessary for plantation-level terrain modeling and hydrological planning (Huang et al., 2023). Second, there is a notable lack of DEM correction frameworks specifically tailored for complex tropical terrain, where elevation errors are amplified by heterogeneous landforms and dense canopy cover (Brock et al., 2020; Chang et al., 2019). Third, while machine learning algorithms such as RF and spatial regression methods like GWR have independently demonstrated value in refining DEM accuracy, few studies have explored their integrated application despite their complementary capabilities. RF is particularly effective at capturing the non-linear relationships between the terrain attributes and the elevation error but lacks spatial sensitivity. Conversely, GWR offers location-specific adaptability by modeling spatial heterogeneity in residuals but is limited in predictive generalization (Kakavas & Nikolakopoulos, 2021; Zhang & Yu, 2022).

To address these limitations, the present study proposes a hybrid DEM correction framework that integrates the global predictive power of RF with the spatial adaptability of GWR to enhance the vertical accuracy of multiple open-source DEMs in a tropical plantation setting. The specific objectives of this research are to: (i) evaluate the vertical accuracy of various open-source DEMs relative to LiDAR-derived elevation data in a complex oil palm plantation environment; (ii) develop and validate an integrated RF-GWR framework for correcting elevation errors; and (iii) identify the most influential terrain-derived predictors associated with vertical discrepancies across diverse topographic conditions.

2. MATERIALS AND METHODS

2.1 Study Area and Gauge Data

This study was conducted in a 39-hectare tropical oil palm plantation in Beluran, Sabah, Malaysia, a region characterized by a tropical rainforest climate with an average annual rainfall of 2,800 mm and temperatures ranging from 25°C to 32°C. The study area features flat

undulating to moderately steep (0^{o} – 24^{o} degrees), making it an ideal environment for evaluating DEM accuracy across varying terrain conditions. To ensure precise elevation validation, 377 GCPs with an average of 9 to 10 GCPs per Hectare were strategically placed across different topographic features, including lowlands, slopes, and ridgelines. GCPs were collected using a CHC i83 GPS GNSS receiver, which provides a horizontal accuracy of 8 mm ± 1 part per million (ppm) and a vertical accuracy of 15 mm ± 1 ppm. The reliability of these GCPs was ensured through differential GPS corrections and cross-validation with LiDAR-derived reference points, minimizing measurement errors before integrating them into the DEM accuracy assessment.

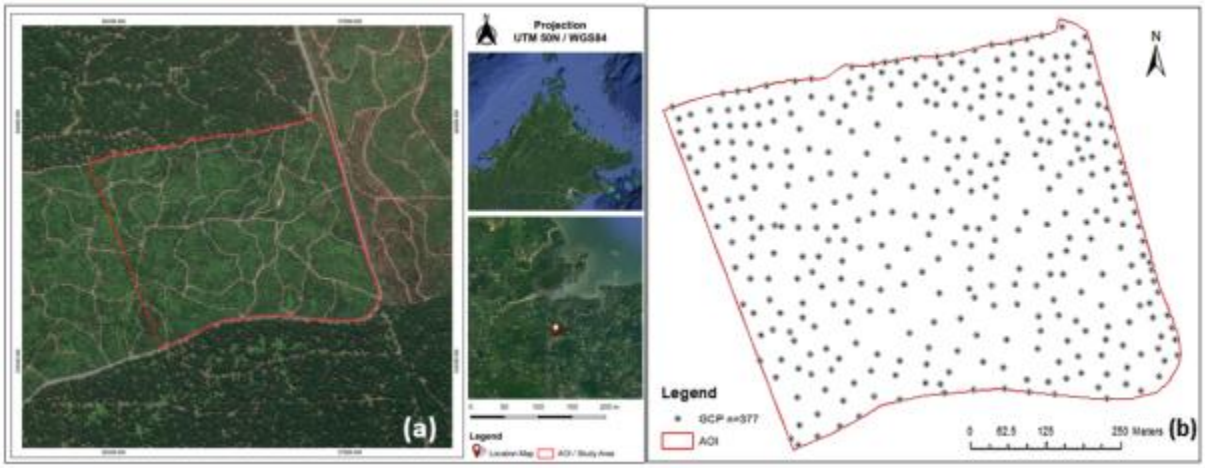

Figure 1: Location of the study area (a) and ground control points (GCPs) (b)

2.2 Open-Source DEMs

This study evaluated the vertical accuracy of several open-source Digital Elevation Models (DEMs) to determine their suitability for terrain analysis in oil palm plantation planning. The DEMs assessed included ALOS World 3D (AW3D30), TanDEM-X, ASTER GDEM, SRTM, Copernicus GLO-30, FABDEM, and a high-resolution Drone RGB-derived DEM obtained via aerial photogrammetry. TanDEM-X and ALOS AW3D30 offer comparatively high vertical accuracy (±2–10 m), whereas ASTER GDEM and SRTM are more susceptible to elevation discrepancies due to vegetation interference and sensor limitations (Rabby et al., 2020). Although Copernicus and FABDEM provide wide global coverage and improved surface representation, their accuracy in complex, heterogeneous terrain remains insufficiently validated (Pareta & Pareta, 2024). The Drone RGB DEM, derived from aerial photogrammetry, delivers a fine spatial resolution but is prone to elevation error caused by surface reflectance and vegetation cover (Scott Watson et al., 2019). For consistency, all DEMs were resampled to a 10 m × 10 m resolution and reprojected to the UTM Zone 50N. Their vertical accuracy was evaluated against both LiDAR-derived elevation data and a set of 377 GCPs. To ensure the reliability of the GCPs, measurements were collected using a CHC i83 GNSS receiver, which offers a horizontal accuracy of ±8 mm ± 1 ppm and a vertical accuracy of ±15 mm ± 1 ppm. Differential GPS corrections and cross-validation with LiDAR reference points were applied to minimize positioning errors, ensuring a robust ground-truth dataset for DEM validation.

Table 1. General information of the DEMs

DEM Source	Acquisition Period	Sensor Type / Processing Method	Vertical Accuracy	Resolution	Datum	Reference
SRTM v3	2000	Radar (C-band InSAR)	±10–16 m	30 m	EGM96 / WGS84	(Uuemaa et al., 2020)
ASTER	2000–2013	Optical (Stereo Imagery)	±8–15 m	30 m	EGM96 / WGS84	(Rabby et al., 2020)
Copernicus	2011–2015	X-band Radar (Reprocessed)	±4–5 m	30 m	EGM2008 / WGS84	(Pareta & Pareta, 2024)
FABDEM	2011–2015	SRTM & Copernicus, with surface object removal	±5–10 m	30 m	EGM2008 / WGS84	(Brochado & Rennó, 2024)
ALOS	2006–2011	Panchromatic Stereo Imagery	±5–10 m	30 m	EGM96 / WGS84	(Tabunshchik et al., 2023)
TanDEM-X	2010–2014	X-band Synthetic Aperture Radar (SAR)	±2–10 m	30 m	EGM96 / WGS84	(Shen et al., 2023)
Drone DEM	Varies	Photogrammetry (DJI Mavic 3 Enterprise RTK)	±5–20 cm	<5 m	GNSS GPS	(Scott Watson et al., 2019)
LiDAR DEM	Varies	Airborne LiDAR	±5–10 cm	<5 m	GNSS GPS	(Chai et al., 2022)

2.3 Terrain Attribute Extraction and Feature Selection

To support the DEM correction, several topographic and terrain-derived attributes were extracted from each dataset. These include elevation, slope, aspect, curvature, TPI and TRI. These variables were chosen based on their proven relevance in influencing elevation error across various terrains, particularly in vegetation-dense and undulating regions. Feature selection was performed using the RF algorithm, which ranks variable importance using two established methods: Mean Decrease in Impurity (MDI) and Mean Decrease in Accuracy (MDA). MDI quantifies the reduction in variance caused by a variable across decision tree splits, while MDA evaluates the decrease in model accuracy when a specific variable is permuted. This dual-ranking approach allowed for a robust identification of the predictors most associated with vertical discrepancies. Across all models, TPI, slope, and curvature consistently emerged as the top contributors to the elevation error. To ensure consistency and comparability across all DEM datasets, the same RF regression parameters were applied throughout the analysis.

2.4 Random Forest and Geographically Weighted Regression (GWR) Models

The JASP open-source software used to run the Random Forest (RF) algorithm was configured with 500 trees (ntree = 500) and three variables randomly selected at each split (mtry = 3). Models were trained on 80% of the ground control point dataset (n = 2,863) and validated on the remaining 20% (n = 715), with out-of-bag (OOB) error used as the internal validation metric. The predictive performance was quantified by the coefficient of determination (R^2) and the root

mean square error (RMSE), representing the explanatory power and predictive accuracy, respectively. To ensure a robust assessment of the variable importance, a permutation-based mean "dropout loss" was computed over 100 permutations. These hyperparameter settings and validation procedures were applied uniformly across all DEM-difference models to maintain the direct comparability of performance metrics and variable-importance rankings. While RF effectively captured the nonlinear relationships between geospatial predictors and elevation error, it did not account for spatial heterogeneity, limiting its capacity to correct location-specific discrepancies. To introduce spatial adaptability, GWR was implemented as a post-processing step. GWR allows regression coefficients to vary across space, thereby modeling localized terrain-error patterns (Kakavas & Nikolakopoulos, 2021; Liu et al., 2020). Residuals from the RF predictions were used as the dependent variable in the GWR framework, enabling locally tuned corrections informed by the landscape's spatial structure. By integrating RF's global predictive strength with GWR's local adaptability, the hybrid approach delivered more accurate and spatially consistent DEM corrections. The final outputs were evaluated against LiDAR-derived elevations and independent GCP measurements to assess the improvements in the vertical accuracy across the DEM sources.

2.5 Methodology

2.5.1 Study Area and Ground Data Collection

The study was carried out within a 39-hectare oil palm plantation in Beluran, Sabah, Malaysia, a region characterized by a tropical rainforest climate with annual rainfall of approximately 2,800 mm and temperatures between 25°C and 32°C. The terrain ranges from flat to moderately steep (0°–24°), offering a suitable gradient for evaluating DEM performance across varying landforms. A total of 377 Ground Control Points (GCPs) were distributed across geomorphological zones including lowlands, slopes, and ridgelines to ensure spatial representativeness. Elevation measurements were obtained using a CHC i83 GNSS receiver (±8 mm horizontal and ±15 mm vertical accuracy), corrected via differential GPS (DGPS) and validated against a LiDAR-derived DEM to ensure high positional accuracy.

2.5.2 Digital Elevation Models (DEMs) and Preprocessing

Seven DEMs were evaluated: ALOS AW3D30, ASTER GDEM v3, Copernicus GLO-30, FABDEM, SRTM v3, TanDEM-X, and a high-resolution drone-derived DEM from aerial photogrammetry. A LiDAR-based DEM served as the benchmark due to its sub-meter vertical accuracy. To ensure spatial consistency, all datasets were resampled to a 10 m × 10 m grid and projected to UTM Zone 50N. Vertical accuracy was assessed by comparing elevation values against both the LiDAR DEM and the 377 GCPs. Metadata and characteristics for each DEM, including resolution, source, and reported accuracy, are summarized in Table 1.

2.5.3 Terrain Attribute Extraction and Feature Selection

To support the elevation error modeling, six terrain attributes including slope, aspect, curvature, Topographic Position Index (TPI), Terrain Ruggedness Index (TRI), and roughness—were derived from the DEMs for use in elevation error modeling. Selection was informed by prior studies highlighting their influence on DEM accuracy in complex terrains. Random Forest (RF) was used to assess predictor importance using Mean Decrease in Impurity (MDI) and Mean

Decrease in Accuracy (MDA). Model hyperparameters, including the number of trees, maximum depth, and minimum samples per leaf, were optimized through grid search and five-fold cross-validation, using RMSE and R^2 as performance metrics.

2.5.4 DEM Error Modeling Using the RF and RF-GWR Hybrid

A two-stage hybrid model was implemented for DEM error correction. In the first stage, RF regression modeled elevation errors based on terrain attributes, with data split into 80% training and 20% testing subsets. While RF effectively captured non-linear terrain-error relationships, it lacked spatial sensitivity. To address this, GWR was applied in the second stage to model RF residuals, using a Gaussian kernel with adaptive bandwidth selected via corrected Akaike Information Criterion (AICc). This spatially adaptive correction improved the model's ability to reflect local elevation variations, resulting in enhanced vertical accuracy across all DEMs.

2.5.5 Model Evaluation and Accuracy Assessment

Model performance was evaluated using standard metrics: the coefficient of determination (R^2) to assess variance explained, root mean square error (RMSE) for prediction accuracy, and residual sum of squares (RSS) for model fit. The spatial kernel bandwidth in GWR was optimized using AICc. Validation was conducted against both the LiDAR DEM and GCP dataset to ensure robustness across varying topographic conditions. In addition to statistical evaluation, spatial residual maps and elevation profiles were generated to visualize model improvements and assess local terrain consistency post-correction.

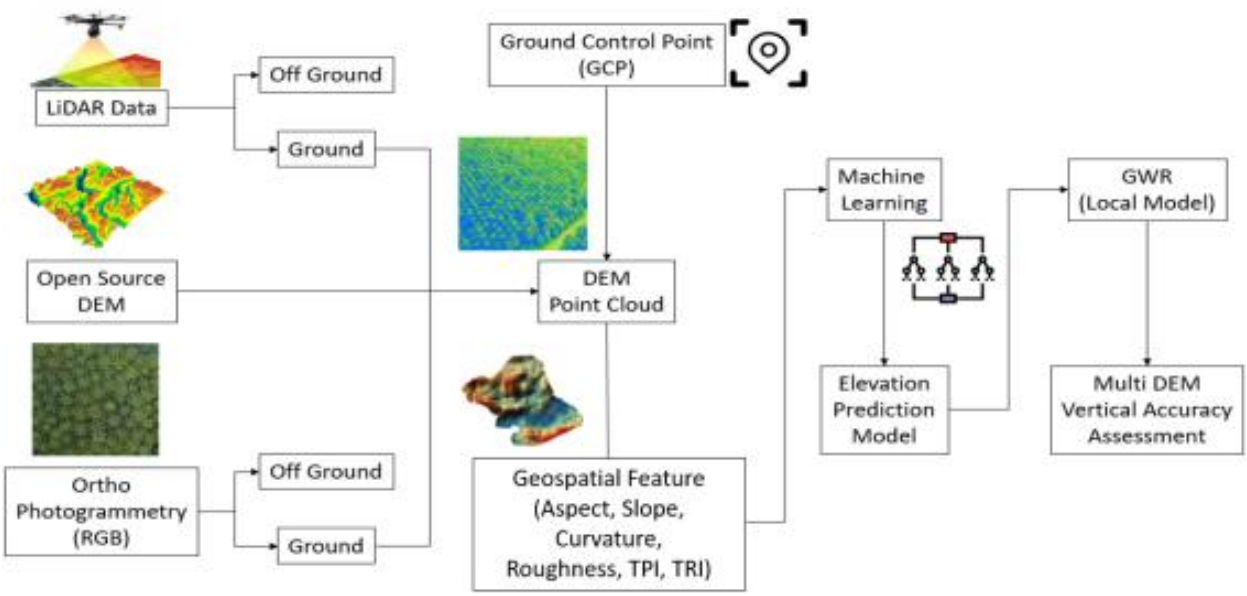

Figure 2: Methodology workflow of the research

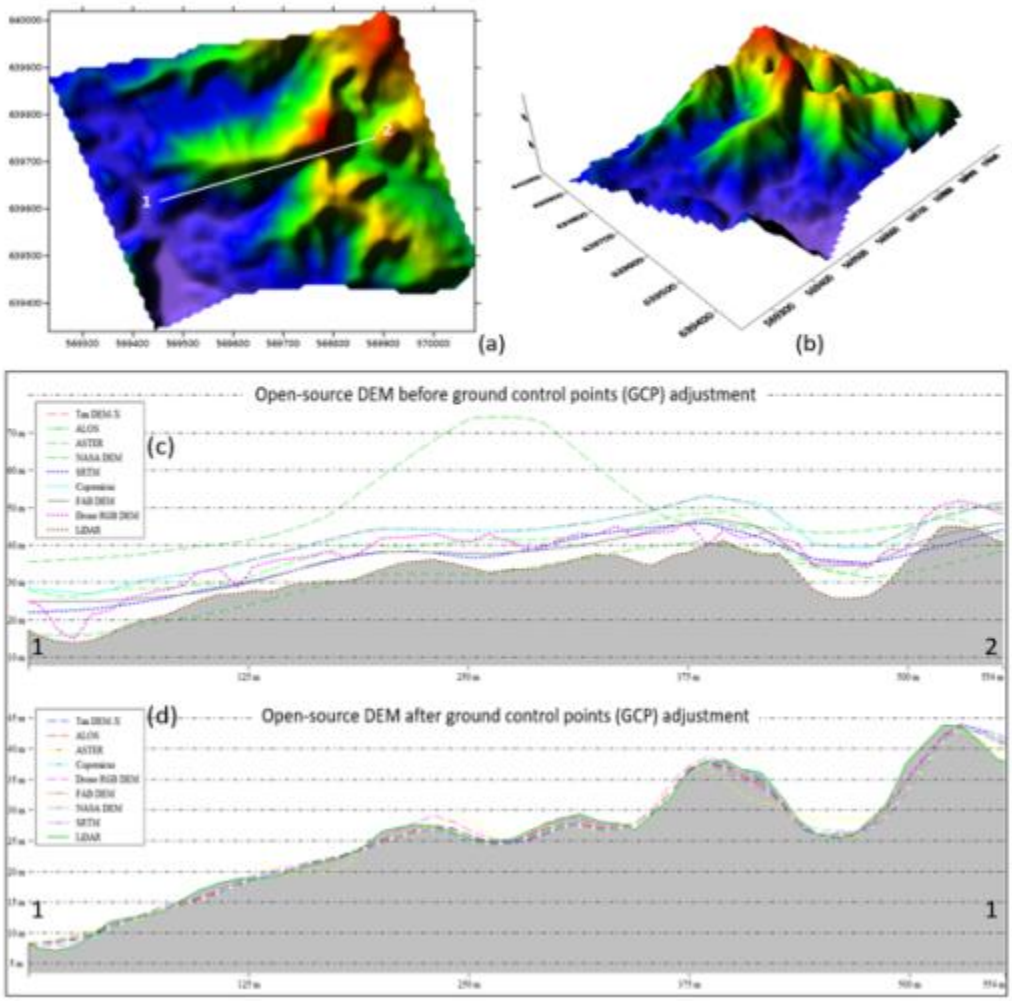

Figure 3: (a) Top-down view of the Digital Elevation Model (DEM), (b) 3D DEM view, and a comparison of the cross-section profile before and after GCPs (c & d)

3. RESULTS

3.1 Influence of Ground Control Points (GCPs) on DEM Accuracy

The initial evaluation revealed substantial discrepancies in the vertical accuracy across uncorrected DEMs, particularly in forested and topographically complex areas. Elevation deviations ranged from 10 to 80 meters when compared with the LiDAR reference, with significant spatial artifacts such as abrupt terrain shifts and slope distortion (Figure 4). These inconsistencies were most pronounced in the steep terrain, where open-source sensors struggled with vegetation occlusion and spatial resolution limitations. Following the integration of 377 high-precision GCPs, the vertical accuracy improved markedly. Post-GCP calibration, the elevation errors were reduced to between 2 and 60 meters across all DEMs. The terrain profiles became smoother, and the elevation transitions were more realistic (Figure 5). This underscores the essential role of ground-truth data in mitigating systematic vertical biases, aligning with the findings of Uuemaa et al., (2020) and demonstrating that even globally available DEMs can be significantly refined with localized calibration.

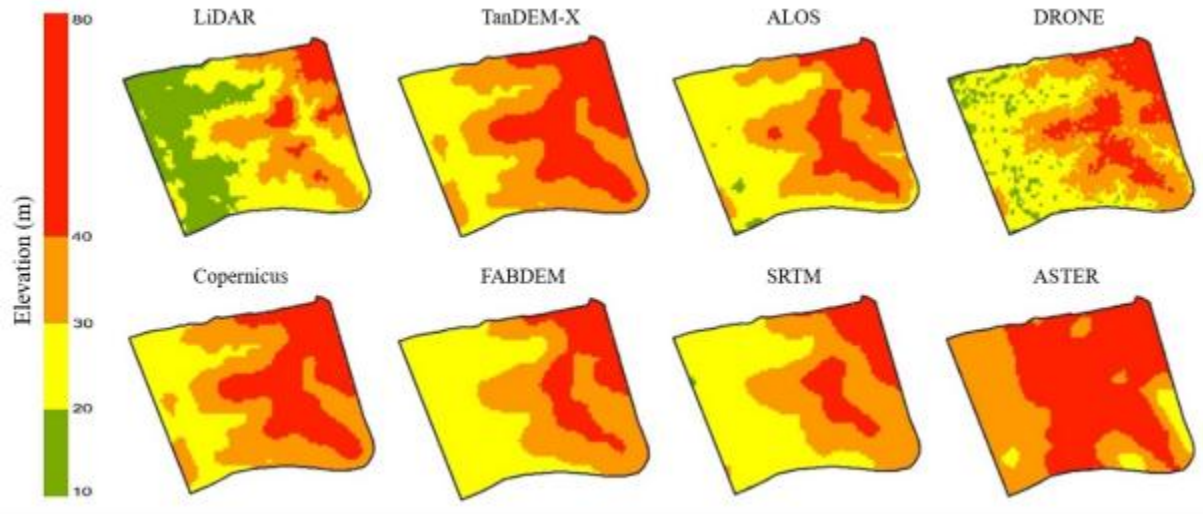

Figure 4: Pre-correction Digital Elevation Models (DEMs)

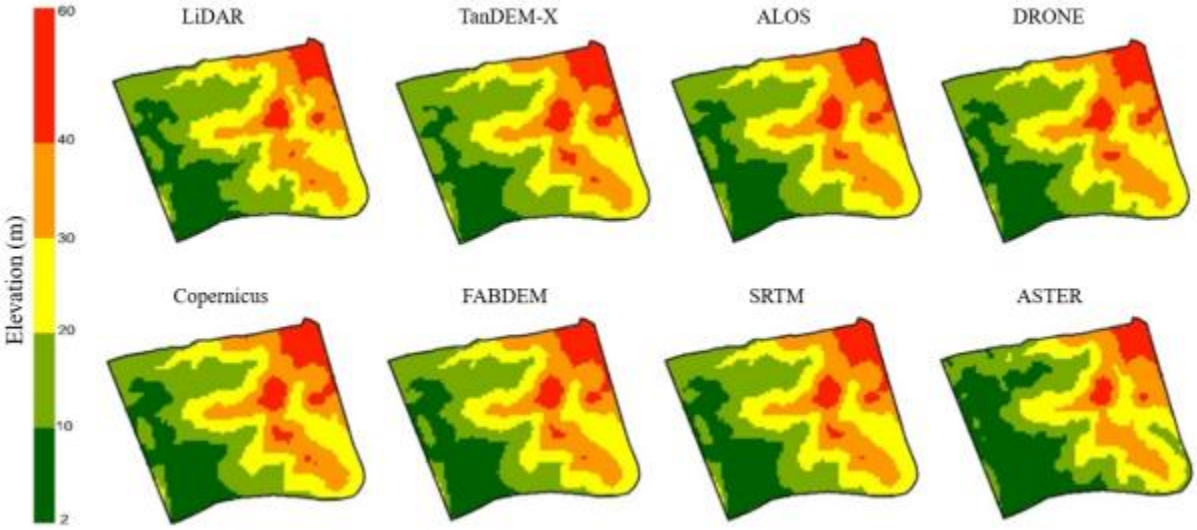

Figure 5: Post-GCP Integrated DEMs

3.2 Random Forest Model Performance in Predicting Elevation Errors

This study provides a comparative assessment of seven DEMs using a Random Forest regression approach to predict elevation errors based on terrain-derived features. The analysis reveals that macro-topographic variables, particularly TPI and curvature, are the most influential predictors of elevation discrepancies across all DEMs. In contrast, aspect consistently contributed the least, underscoring its limited role in error modeling at broader spatial scales. As show in table 2 below, Copernicus DEM emerged as the best overall performer (R^2 = 0.608), while ALOS achieved the highest accuracy (lowest RMSE = 0.722). Conversely, ASTER GDEM showed significantly weaker predictive capability, reaffirming known issues with vegetation-induced

distortions. The results demonstrate that while Random Forest models effectively reduce broad-scale elevation biases, they require augmentation with additional environmental variables (e.g., land cover, canopy height) to capture fine-scale variation. This emphasizes the need for hybrid approaches that integrate the DEM structure with contextual surface data for robust elevation error correction.

Table 2: Comparative performance of DEMs in predicting elevation errors using random forest and geospatial feature predictors

DEM	R^2	RMSE	Predictors (Most Predictive to Least Predictive)
ALOS	0.589	0.722	TPI, Curvature, TRI, Roughness, Slope, Aspect
ASTER	0.521	1.125	TPI, Curvature, TRI, Roughness, Slope, Aspect
Copernicus	0.608	0.786	TPI, Curvature, Roughness, TRI, Slope, Aspect
Drone	0.569	0.815	TPI, Curvature, TRI, Roughness, Slope, Aspect
FABDEM	0.572	0.857	TPI, Curvature, TRI, Slope, Roughness, Aspect
SRTM	0.571	0.897	TPI, Curvature, TRI, Roughness, Slope, Aspect
TanDEM-X	0.588	0.820	TPI, Curvature, TRI, Roughness, Slope, Aspect

3.3 Performance of the Hybrid RF–GWR Models Across DEMs

In this study, a hybrid modeling framework was employed by integrating RF prediction with GWR. The residuals (or predictions) from the RF model served as the dependent variable in the GWR, enabling the spatial dissection of the terrain to influence the prediction performance. This approach allowed for both high-accuracy predictions via machine learning and spatial diagnostics through geographically localized regression. Table 3 summarizes the diagnostic metrics of the hybrid RF+GWR models across seven DEMs. The models varied in performance based on AIC, corrected AIC (AICc), residual sum of squares (RSS), and R^2 statistics.

Table 3: Comparing the hybrid RF+GWR model results across the different DEM using the Random Forest prediction

DEM	AIC	AICc	RSS	R^2	Adj. R^2	Top GWR Predictor (by Median Coefficient)
TanDEM-X	1999.50	2476.73	329.16	0.914	0.898	TPI (Median = 2.063)
SRTM	2625.04	3282.26	379.92	0.913	0.892	TPI (Median = 2.153)
FABDEM	2477.94	2955.48	376.23	0.906	0.889	TPI (Median = 2.121)
DRONE	1753.73	2220.05	307.93	0.910	0.894	TPI (Median = 1.817)
COPERNICUS	1852.73	2330.51	315.90	0.914	0.898	TPI (Median = 1.940)
ASTER	3643.63	4300.00	505.12	0.905	0.883	TPI (Median = 2.122)
ALOS	1065.85	1539.07	253.75	0.910	0.894	TPI (Median = 1.932)

* AIC = Akaike Information Criterion & * AICc = Akaike Information Criterion corrected

The ALOS-based hybrid model demonstrated the best overall performance, achieving the lowest AIC (1065.85), lowest AICc (1539.07), and smallest RSS (253.75), with a high adjusted R^2 value of 0.8940. These results suggest that the terrain derivatives derived from the ALOS data are

particularly effective in explaining the spatial variation in the RF residuals. Close contenders included the DRONE and COPERNICUS-based models, which also achieved high adjusted R^2 values of 0.8943 and 0.8988, respectively, and maintained relatively low AIC scores. In contrast, the ASTER-based hybrid model exhibited the weakest performance, with the highest AICc (4300.00), the largest RSS (505.12), and the lowest adjusted R^2 (0.8830) among all DEMs. These results may reflect the known limitations of ASTER in terms of vertical accuracy and resolution, which likely affect the reliability of its derived terrain metrics in localized spatial analysis. Across all hybrid models, the TPI consistently emerged as the most influential topographic predictor, based on the median GWR coefficients. The SRTM model recorded the highest TPI median value (2.153), followed closely by ASTER (2.122), FABDEM (2.121), and TanDEM-X (2.063). Even in models with lower overall performance, the TPI retained its dominant influence. This consistent pattern indicates that landscape position features (e.g., valleys, ridges, flat zones) have the strongest and most stable spatial correlation with the RF prediction outcomes, regardless of the DEM source. TPI's prominence suggests it captures critical geomorphological variations that strongly influence the spatial structure of model errors or predictions. Other variables, such as curvature, slope, roughness, and TRI, showed more variability across the DEMs and had lower median coefficients. The curvature was typically negative, suggesting that concave or convex terrain forms may negatively impact the RF prediction accuracy. Roughness and TRI contributed moderately but inconsistently across the models.

3.4 Residual Error Analysis Across Modeling Approaches

Table 4 presents the descriptive statistics of the residual errors for the seven digital elevation models (DEMs), evaluated using three modeling approaches: (i) uncorrected residuals from the raw DEMs, (ii) residuals from the random forest (RF) regression, and (iii) residuals from a hybrid model combining the random forest with the geographically weighted regression (RF+GWR). Residuals were computed as the difference between the DEM-predicted elevations and the GCPs benchmark elevations.

Table 4: Residual error statistics for the raw, RF, and RF+GWR Models

DEM	Mean	Std. Deviation	Minimum	Maximum
Residual ALOS	0.041	1.135	-5.134	7.163
Residual ASTER	0.050	1.627	-8.564	10.55
Residual COPERNICUS	0.019	1.272	-6.185	6.284
Residual DRONE	-0.008	1.216	-7.550	6.314
Residual FABDEM	0.053	1.334	-5.735	8.124
Residual SRTM	0.074	1.399	-5.858	8.792
Residual TAN DEM-X	0.030	1.293	-5.686	8.343
Residual RF ALOS	0.043	0.901	-3.417	4.459
Residual RF ASTER	0.057	1.225	-5.768	7.524
Residual RF COPERNICUS	0.019	1.015	-4.500	4.033
Residual RF DRONE	-0.003	0.979	-4.447	3.714
Residual RF FABDEM	0.058	1.062	-3.966	5.028

Residual RF SRTM	0.078	1.106	-4.168	5.630
Residual RF TanDEM-X	0.034	1.035	-3.85	4.950
Residual RF+GWR ALOS	-97.81	0.266	-1.246	1.119
Residual RF+GWR ASTER	-0.001	0.376	-1.784	1.966
Residual RF+GWR Copernicus	0.002	0.306	-1.747	1.169
Residual RF+GWR DRONE	0.002	0.293	-1.827	1.17
Residual RF+GWR FABDEM	-52.16	0.324	-1.547	1.402
Residual RF+GWR SRTM	-0.002	0.326	-1.533	1.711
Residual RF+GWR TanDEM-X	0.001	0.303	-1.344	1.321

Across all DEMs, the raw residuals exhibited the highest variability, with standard deviations ranging from 1.135 (ALOS) to 1.627 (ASTER). Most DEMs also showed positive mean residuals, indicating a tendency to overestimate elevation. For instance, the ASTER model had a mean residual of 0.050 m and a maximum residual of over 10.5 m, suggesting a significant vertical error and high spread. Applying the Random Forest regression led to a substantial improvement in the model performance. All DEMs showed a marked reduction in the standard deviation, indicating enhanced precision. For example, the standard deviation of the FABDEM residuals decreased from 1.334 to 0.972. The mean residuals also approached zero, suggesting a reduced bias. The RF model consistently outperformed the raw DEMs, demonstrating its effectiveness in learning terrain-related error patterns. The hybrid RF+GWR model further refined the residual accuracy. It consistently achieved the lowest standard deviations (e.g., 0.303 for TanDEM-X, 0.306 for Copernicus) and mean residuals nearly equal to zero, indicating minimal spatial bias and high local accuracy. Notably, the hybrid approach reduced the standard deviation of the FABDEM residuals from 0.972 (RF-only) to 0.324, underscoring the value of incorporating spatial heterogeneity through the GWR. In summary, the hybrid RF+GWR approach outperformed both the raw DEMs and the RF-only models, producing the most accurate and spatially consistent elevation estimates. These findings support the integration of spatial regression into machine learning workflows to enhance DEM correction and surface modeling accuracy.

4. DISCUSSION

The integration of RF and GWR provides a robust framework for enhancing the vertical accuracy of DEMs in a complex tropical landscape. The findings demonstrate that the RF–GWR model effectively reduces systematic and spatially variable elevation errors, resulting in substantial improvements across all evaluated DEM products. The hybrid model yielded particularly strong performance in TanDEM-X and ALOS datasets, with post-correction R^2 values exceeding 0.91 approaching the precision of LiDAR-derived elevation models. Similarly, the Copernicus GLO-30 DEM exhibited the greatest relative enhancement, with R^2 improving from 0.608 to 0.914 These results affirm the suitability of the RF–GWR approach for terrain-sensitive applications and support previous findings that emphasize the importance of combining data-driven learning with spatially adaptive techniques to correct elevation biases (Dong et al., 2020; Yu et al., 2021; Zhang & Yu, 2022).

The model's success can be further contextualized within a wider framework of literature that highlights the role of local terrain attributes in shaping DEM error patterns. The consistent identification of topographic predictors particularly TPI, slope, and curvature aligns with prior studies on elevation modeling in forested and mountainous terrain (Mishra et al., 2021; Zhang & Yu, 2022). While the RF model effectively captured the nonlinear relationships between these predictors and elevation error, its inability to account for spatial autocorrelation in complex terrain was addressed through the incorporation of GWR. The spatial variation of regression coefficients in the GWR model enabled more nuanced, location-specific corrections, leading to smoother residual patterns and improved local accuracy (Amelia et al., 2023; Li, 2022).

Notwithstanding its strengths, several limitations should be acknowledged. First, the framework is reliant on high-quality GCPs for calibration and validation. In regions where such data are sparse or difficult to acquire, model accuracy may be compromised. This constraint presents logistical and financial challenges for large-scale deployment or community-led mapping initiatives (Mehra & Swain, 2024; Yu et al., 2021). Second, the GWR component is computationally intensive, potentially limiting real-time scalability and cloud-based implementation without further optimization (Al-Nasrawi et al., 2021; Ganju et al., 2020). Lastly, the model is temporally static and does not account for landscape dynamics such as seasonal vegetation shifts, land-use changes, or erosion, which may affect DEM accuracy over time (Hu et al., 2024).

Future research should therefore prioritize several directions. The integration of advanced machine learning algorithms such as Extreme Gradient Boosting (XGBoost) or Convolutional Neural Networks (CNNs) may further improve predictive accuracy and computational efficiency (Dumarevskaya & Parent, 2025). In parallel, geostatistical interpolation methods such as kriging could be incorporated to complement the RF–GWR model, offering finer control over spatial prediction (Idrissi et al., 2023). Finally, the development of cloud-based, real-time correction workflows leveraging open-access Earth observation data would support operational use cases such as flood forecasting, terrain planning, and precision agriculture, particularly in geospatially constrained environments (Baldarelli et al., 2024; Zamora-Espinoza et al., 2024).

5. CONCLUSION

This study presents a hybrid modeling framework that integrates RF with GWR to correct elevation inaccuracies in open-source DEMs within a tropical oil palm plantation context. Using a robust dataset of 377 high-precision GCPs and LiDAR-derived reference surfaces, the framework was applied to six global DEM products and one drone-derived model. The results demonstrated significant improvements in vertical accuracy, with post-correction R^2 values reached 0.914 for TanDEM-X, 0.910 for ALOS, and a notable increase for Copernicus GLO-30 from 0.608 to 0.914. These findings underscore the effectiveness of combining machine learning with spatial regression to address both systematic and localized elevation errors in complex landscapes. The model offers a scalable, cost-effective alternative to LiDAR for elevation modeling tasks in resource-constrained settings and provides practical value for precision agriculture, hydrological planning, and environmental monitoring. The proposed framework not only improves prediction performance but also captures spatial heterogeneity more effectively than single-method approaches. It is recommended that future research extend this framework through the integration of temporal datasets, enabling dynamic monitoring of terrain changes.

Additionally, deploying the model in cloud environments and incorporating newer machine learning algorithms can further enhance its operational scalability. These advancements will be instrumental in supporting real-time decision-making and adaptive land management across diverse and data-limited geographies. In summary, the RF–GWR hybrid model constitutes a valuable contribution to the field of digital terrain analysis, offering both methodological innovation and practical applicability in enhancing the accuracy of globally accessible elevation datasets.

ACKNOWLEDGMENT

The authors express their heartfelt gratitude to colleagues, Freddyson Boak @ Matiu, Haiddy Dahalan, Mohd. Nur Azizi Bin Aziz and Ronald Daimel for their invaluable contributions of technical assistance and unwavering support throughout this research project.

REFERENCE

Al-Nasrawi, A. K. M., Kadhim, A. A., Shortridge, A. M., & Jones, B. G. (2021). *Accounting for dem error in sea level rise assessment within riverine regions; case study from the shatt al-arab river region.* Environments - MDPI, 8(5), 46. https://doi.org/10.3390/environments8050046

Amelia, V., Sinaga, S., & Bhermana, A. (2023). *Land resource management on environment and sustained basis for agricultural land use planning using landform and land evaluation approach (a case study in North Barito District, Central Kalimantan Province)*. IOP Conference Series: Earth and Environmental Science, 1282(1), 12001. https://doi.org/10.1088/1755-1315/1282/1/012001

Baldarelli, L. M., Ward, D., & Throop, H. L. (2024). *Elevation and parent material drive biocrust distributions and soil extracellular enzyme activity along a dryland elevation gradient.* https://doi.org/10.21203/rs.3.rs-3861531/v1

Brochado, G. T., & Rennó, C. D. (2024). *New Method to Correct Vegetation Bias in a Copernicus Digital Elevation Model to Improve Flow Path Delineation*. Remote Sensing, 16(22). https://doi.org/10.3390/rs16224332

Brock, J., Schratz, P., Petschko, H., Muenchow, J., Micu, M., & Brenning, A. (2020). *The performance of landslide susceptibility models critically depends on the quality of digital elevations models.* Geomatics, Natural Hazards and Risk, 11(1), 1075–1092. https://doi.org/10.1080/19475705.2020.1776403

Chai, L. T., Wong, C. J., James, D., Loh, H. Y., Liew, J. J. F., Wong, W. V. C., & Phua, M. H. (2022). *Vertical accuracy comparison of multi-source Digital Elevation Model (DEM) with Airborne Light Detection and Ranging (LiDAR)*. IOP Conference Series: Earth and Environmental Science, 1053(1), 012025. https://doi.org/10.1088/1755-1315/1053/1/012025

Chang, K.-T., Merghadi, A., Yunus, A. P., Pham, B. T., & Dou, J. (2019). *Evaluating scale effects of topographic variables in landslide susceptibility models using GIS-based machine learning techniques.* Scientific Reports, 9(1), 12296. https://doi.org/10.1038/s41598-019-48773-2

Dong, G., Huang, W., Smith, W. A. P., & Ren, P. (2020). *Filling Voids in Elevation Models Using a Shadow-Constrained Convolutional Neural Network.* IEEE Geoscience and Remote Sensing Letters, 17(4), 592–596. https://doi.org/10.1109/LGRS.2019.2926530

Dumarevskaya, L., & Parent, J. R. (2025). *Modeling Spongy Moth Forest Mortality in Rhode Island Temperate Deciduous Forest.* Forests, 16(1), 93. https://doi.org/10.3390/f16010093

Ganju, N. K., Defne, Z., & Fagherazzi, S. (2020). Are Elevation and Open-Water Conversion of Salt Marshes Connected? Geophysical Research Letters, 47(3). https://doi.org/10.1029/2019GL086703

Hu, H., Zhou, H., Cao, K., Lou, W., Zhang, G., Gu, Q., & Wang, J. (2024). *Biomass Estimation of Milk Vetch Using UAV Hyperspectral Imagery and Machine Learning.* Remote Sensing, 16(12), 2183. https://doi.org/10.3390/rs16122183

Huang, J., Wei, L., Chen, T., Luo, M., Yang, H., & Sang, Y. (2023). *Evaluation of DEM Accuracy Improvement Methods Based on Multi-Source Data Fusion in Typical Gully Areas of Loess Plateau.* Sensors, 23(8), 3878. https://doi.org/10.3390/s23083878

Idrissi, I. C. E., Nouh, S., Bellfkih, E. M., Marzak, A., & El Assad Assad, M. (2023). *Error-Correcting Codes and the Power of Machine Learning: Enhancing Data Reliability.* In Proceedings - SITA 2023: 2023 14th International Conference on Intelligent Systems: Theories and Applications. https://doi.org/10.1109/SITA60746.2023.10373727

Kakavas, M. P., & Nikolakopoulos, K. G. (2021). *Digital Elevation Models of Rockfalls and Landslides: A Review and Meta-Analysis.* Geosciences, 11(6), 256. https://doi.org/10.3390/geosciences11060256

Karlson, M., Bastviken, D., & Reese, H. (2021). *Error Characteristics of Pan-Arctic Digital Elevation Models and Elevation Derivatives in Northern Sweden.* Remote Sensing, 13(22), 4653. https://doi.org/10.3390/rs13224653

Li, Z. (2022). *Extracting spatial effects from machine learning model using local interpretation method: An example of SHAP and XGBoost.* Computers, Environment and Urban Systems, 96(June), 101845. https://doi.org/10.1016/j.compenvurbsys.2022.101845

Liu, C., Li, W., Zhu, G., Zhou, H., Yan, H., & Xue, P. (2020). *Land use/land cover changes and their driving factors in the northeastern tibetan plateau based on geographical detectors and google earth engine: A case study in gannan prefecture*. Remote Sensing, 12(19). https://doi.org/10.3390/RS12193139

Martinez, A. (2020). *Using Terrain Algorithms on a Digital Elevation Model to Evaluate Yield Variability in Oil Palm*. Journal of Oil Palm Research, 33(1), 84–92. https://doi.org/10.21894/jopr.2020.0092

Mehra, N., & Swain, J. B. (2024). *Geospatial Assessment of Urban Sprawl Using Remote Sensing and GIS: A Case Study of Western Himalayan City of Dharmashala, Himachal Pradesh, India.* IOP Conference Series: Earth and Environmental Science, 1327(1), 012031. https://doi.org/10.1088/1755-1315/1327/1/012031

Mishra, U., Hugelius, G., Shelef, E., Yang, Y., Strauss, J., Lupachev, A., Harden, J. W., Jastrow, J. D., Ping, C. L., Riley, W. J., Schuur, E. A. G., Matamala, R., Siewert, M., Nave, L. E., Koven, C. D., Fuchs, M., Palmtag, J., Kuhry, P., Treat, C. C., … Orr, A. (2021). S*patial heterogeneity and environmental predictors of permafrost region soil organic carbon stocks.* Science Advances, 7(9). https://doi.org/10.1126/sciadv.aaz5236

Mohamed, M. (2020). *Classification of Landforms for Digital Soil Mapping in Urban Areas Using LiDAR Data Derived Terrain Attributes: A Case Study from Berlin, Germany*. Land, 9(9), 319. https://doi.org/10.3390/land9090319

Pareta, K., & Pareta, U. (2024). *Evaluation of stream ordering systems in the context of topography and open-source data.* Earth Surface Processes and Landforms, 49(12), 3806–3821. https://doi.org/10.1002/esp.5938

Rabby, Y. W., Ishtiaque, A., & Rahman, M. S. (2020). *Evaluating the effects of digital elevation models in landslide susceptibility mapping in rangamati district, Bangladesh.* Remote Sensing, 12(17), 2718. https://doi.org/10.3390/RS12172718

Scott Watson, C., Kargel, J. S., & Tiruwa, B. (2019). *Uav-derived himalayan topography: Hazard assessments and comparison with global dem products.* Drones, 3(1), 1–18. https://doi.org/10.3390/drones3010018

Shen, X., Zhou, C., & Zhu, J. (2023). *Improving the Accuracy of TanDEM-X Digital Elevation Model Using Least Squares Collocation Method*. Remote Sensing, 15(14), 3695. https://doi.org/10.3390/rs15143695

Tabunshchik, V., Gorbunov, R., Gorbunova, T., Pham, C. N., & Klyuchkina, A. (2023). *Identification of river basins within northwestern slope of Crimean Mountains using various digital elevation models (ASTER GDEM, ALOS World 3D, Copernicus DEM, and SRTM DEM)*. Frontiers in Earth Science, 11. https://doi.org/10.3389/feart.2023.1218823

Tavares da Costa, R., Mazzoli, P., & Bagli, S. (2019). *Limitations Posed by Free DEMs in Watershed Studies: The Case of River Tanaro in Italy.* Frontiers in Earth Science, 7. https://doi.org/10.3389/feart.2019.00141

Uuemaa, E., Ahi, S., Montibeller, B., Muru, M., & Kmoch, A. (2020). *Vertical accuracy of freely available global digital elevation models (Aster, aw3d30, merit, tandem-x, srtm, and nasadem).* Remote Sensing, 12(21), 1–23. https://doi.org/10.3390/rs12213482

Yu, W., Bain, R. E. S., Yu, J., Alegana, V., Dotse-Gborgbortsi, W., Lin, Y., & Wright, J. A. (2021). *Mapping access to basic hygiene services in low- and middle-income countries: A cross-sectional case study of geospatial disparities*. Applied Geography, 135, 102549. https://doi.org/10.1016/j.apgeog.2021.102549

Zamora-Espinoza, A., Chin, J., Quesada-Román, A., & Obando, V. (2024). *Geospatial Approach to Determine Nitrate Values in Banana Plantations*. AgriEngineering, 6(3), 2513–2525. https://doi.org/10.3390/agriengineering6030147

Zhang, Y., & Yu, W. (2022). *Comparison of DEM Super-Resolution Methods Based on Interpolation and Neural Networks.* Sensors, 22(3), 745. https://doi.org/10.3390/s22030745